Stability Analysis for Large Signal Design of a Microwave Frequency Doubler

Saswata Basu, Stephen A. Maas, *Fellow, IEEE*, and Tatsuo Itoh, *Fellow, IEEE*

***Abstract*—Microwave circuits such as frequency doublers are notorious for instabilities under parametric variation. The instabilities manifested in the doubler are due to the minority carrier lifetime of the *pn* junction diode. They are calculated using a simpler stability formulation. A global stability chart is computed using a novel technique called the piecewise stability analysis (PSA) method and found to be in close agreement with the experimental values. These instabilities are characterized by secondary Hopf bifurcations and their eventual breakdown to chaos has been observed. The onset of Hopf bifurcation has been verified both experimentally and numerically.**

I. Introduction

THE LARGE SIGNAL DESIGN of frequency doublers is made difficult by the appearance of chaotic instabilities at higher power or bias levels [1]. This type of instability is also existent in step-recovery diodes [2]. No work has been done previously on predicting such instabilities accurately. In this paper, we predict the onset of these spurious oscillations. It is found that these oscillations disintegrate to chaos with parametric variation of the bias and/or input power levels. The oscillations in the varactor doubler is caused by the dynamically negative resistance manifested in the *pn* junction diode. The cause of the spurious oscillations in the doubler is verified through numerical simulation and an experiment.

The negative resistance effect of a junction diode has been studied earlier in the 1960s under the topic of parametric amplification [3]. However, this parametric effect is different from the work discussed here in the sense that a pump frequency and a small-amplitude signal frequency are simultaneously applied to make the device behave like a time-varying linear capacitance at the signal frequency. When the current is permitted to exist at the idler frequency $\omega_p - \omega_s$, further mixing occurs and results in a power transfer from the pump signal to the RF signal which is interpreted as an equivalent negative resistance.

The prediction of these instabilities is based on the stability formulation derived through the perturbation approach in frequency domain, very similar to the approach taken in [4], [5], but considerably simpler and practical. The stability analysis is coupled with bifurcation theory and chaos theory to predict and explain the physical behavior of the doubler under a parametric variation. This one-parameter stability analysis can be extended to more than one parameter variation. Multi-parameter stability charts provide useful design information such as stability regions of operation for a frequency doubler with bias and input power variations. These variations are likely to occur in practice due to temperature changes, time delay of other components associated with the doubler, or manufacturer tolerance. However, the computational effort required is extensive since the admittance parameters of the linear subcircuit need to be recalculated everytime a parameter in the circuit is changed. In this work, a technique called the piecewise stability analysis has been devised to avoid such repetetive computations.

We start first by discussing some observations of chaotic instability in the frequency doubler.

Manuscript received March 1, 1995; revised July 10, 1995.
S. Basu is with Cascade Microtech, Inc., Beaverton, OR 97005 USA.
T. Itoh is with the University of California, Los Angeles, CA USA.
S. A. Maas is with Nonlinear Technologies Inc., Long Beach, CA USA.
IEEE Log Number 9415444.

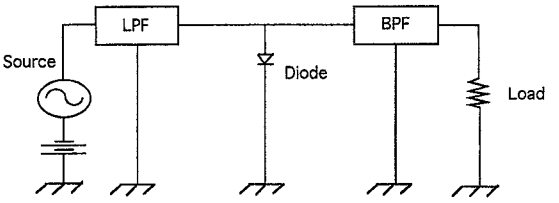

Fig. 1. A block diagram view of a microwave doubler circuit.

II. Observation of Chaos

The *pn* junction diode used in the paper is an Alpha DVA6735-06 silicon varactor diode. The doping profile is typical of an abrupt junction diode with a doping density/cm^3 of 10^{21} for p^+ diffused, 10^{16} for n epi-layer and 10^{19} for n^+ substrate.

Chaos has been observed in various low frequency circuits and mechanical systems [6], Gunn oscillators [7], and microwave limiters [8]. The path of chaos can be through the period doubling, period adding, intermittent, or quasi-periodic routes depending on the system. In the doubler, only the quasi-periodic route is observed.

Fig. 1 depicts a block diagram of a microwave doubler circuit. It consists of a low pass filter at 5 GHz, a bandpass filter at 10 GHz, and a *pn* junction diode to provide harmonic generation; the bias and tuning elements are not shown in the diagram for the sake of clarity. The bias line has a narrowband RF rejection at the input frequency and, therefore, allows for perturbation at other frequencies. The input signal to the doubler is held fixed at 16 dBm and the bias is varied from -3.0 V to 0.0 V. At the low end of the bias, the doubler is in normal mode of operation; no bifurcation is displayed. As the bias level is increased, the doubler exhibits Hopf

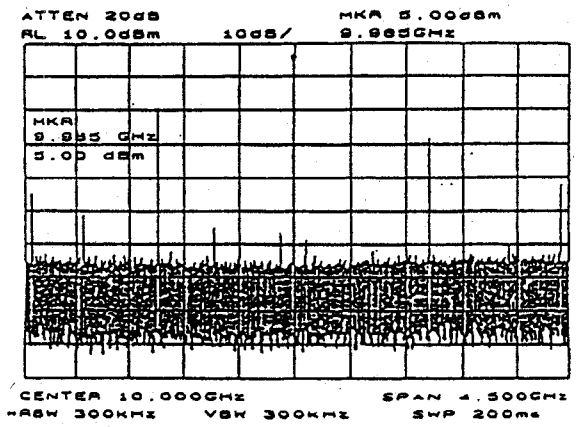

(a)

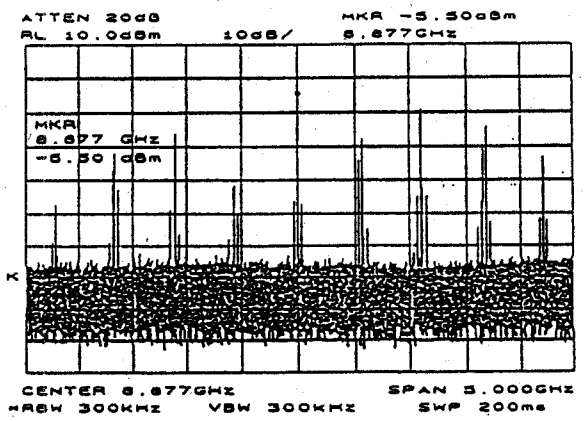

(b)

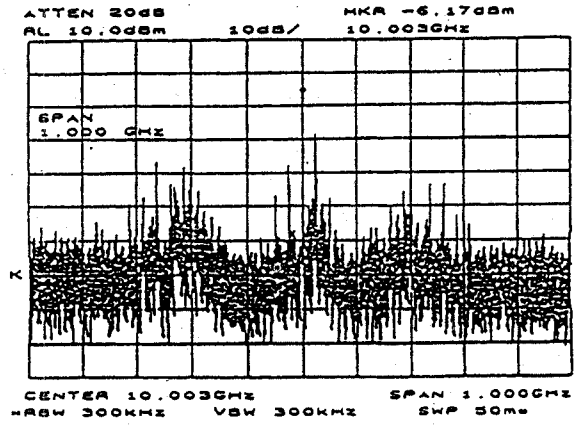

(c)

Fig. 2. A spectral portrait of frequency doubler in different states with increasing bias levels: (a) two-frequency quasi-periodic, (b) three-frequency quasi-periodic, and (c) chaos.

bifurcation and mixes with the input frequency as depicted in Fig. 2(a). Increasing the bias level further, the magnitude of the oscillation increases gradually until it reaches a point when, suddenly, the regime bifurcates into a three-frequency quasi-periodic state as shown in Fig. 2(b). The three-frequency regime, vulnerable to external perturbations, breaks down to chaos as shown in Fig. 2(c). The chaotic state is manifested by a broadband spectrum around the mixing product spectral lines. Increasing the bias level further suppresses the chaotic state allowing the return of the two-frequency quasi-periodic regime.

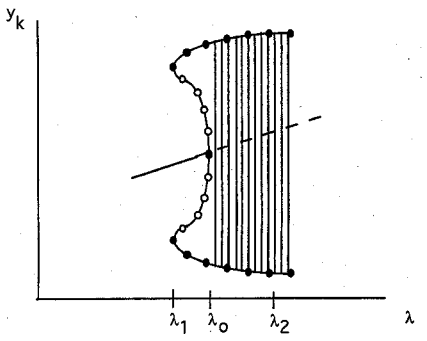

Fig. 3. A Hopf bifurcation with a hard loss of stability.

The initial loss of stability is brought about in a "soft" manner; that is, the amplitude of oscillation increases slowly from the Hopf bifurcation point. The next loss of stability is brought about in a "hard" manner. The oscillation resulting from the secondary Hopf bifurcation is not stable and it goes through a turning point before jumping onto the stable branch of the oscillation as conceptually elucidiated in Fig. 3 [9]. A heavy continuous line represents stable stationary solutions, and a dashed line indicates unstable stationary solutions. A filled dot at an intersection between lines marks a branch point; in this case, it is a Hopf bifurcation point. Filled dots on a line represent stable periodic solutions, whereas transparent dots stand for unstable periodic solutions. In the diagram, $y(t)$ is a n-dimensional vector and, for the sake of presenting the amplitude of oscillation with parametric variation, one maximum and one minimum of $y_k(t)$ is depicted. To numerically replicate these experimental observations, an expensive multitone stability analysis is required and is not pursued in this work.

A. Explanation of Chaos

Hunt's [10] explanation of the occurence of chaos in a simple RLC driven circuit containing a *pn* junction diode as its nonlinear element has been confirmed through numerical computations of state equations [11]. The chaos in his circuit was preempted by the period doubling route and follows a classic bifurcation tree pattern, which can be generated through simple logistic equations. A similar explanation holds for the chaos we have observed in the microwave doubler, although here due to a different linear circuitry the chaotic route happens to be quasi-periodic unlike the period doubling observed in [10].

The *pn* junction diode has a finite recombination lifetime. When the diode is switched from the forward biased to the reverse biased mode, it still conducts in the same direction due to the presence of minority carriers which do not have enough time to recombine with relative speed of the input signal. This delay gives rise to a dynamical negative resistance, which grows with increased bias level. The negative resistance sets

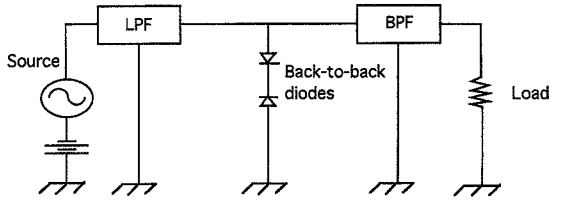

Fig. 4. A back-to-back two-diode nonbifurcating frequency doubler circuits.

up a regime where Hopf bifurcation occurs. This fact has been experimentally tested in [12] using fast signal diodes, where no bifurcation was observed. In addition, it is well known that doublers based on majority carrier nonlinear devices such as Schottky barrier diodes do not exhibit bifurcations. The input signal and the oscillation frequency sets up a two-frequency quasi-periodic regime. With increased bias level another Hopf bifurcation follows resulting in a three-frequency quasi-periodic regime. At this stage, chaos becomes likely to occur from external perturbations. This fact has been mathematically proven for generic systems and experimentally observed by Ruelle and Takens [13]. According to the Ruelle and Takens scenario, the torus may breakdown to chaos or may metamorphize to a three-frequency quasi-periodic regime before chaos depending on the system. In our case, the latter phenomenon has been observed.

B. Experimental Verification

The chaotic doubler circuit in Fig. 1 was slightly modified by incorporating an additional diode in a back-to-back series connected fashion as depicted in Fig. 4. The choice of the anode or cathode of the diodes facing outward in the back-to-back structure is not relevant to the experiment and will give similar results. In this structure one of the diodes stay reverse-biased all the time. Because of the series connection the structure is never in the forward biased mode. Consequently, there is no recombination time delay effect and hence, spurious oscillations were not observed.

The back-to-back doubler still provides a conversion, but not as good as a single-diode doubler. The conversion results from the nonlinearity of the charge or capacitance of the two diodes. The C-V curves of the two diodes, one forward biased, the other reverse biased, and their combined effect are shown in Fig. 5. At the built-in potential, the capacitance of the forward biased diode approaches infinity due to the closure of the depletion region. The combined series capacitance becomes essentially that of the reverse biased diode. At zero volts, the total capacitance is half that of a single diode. As a result, the variation of capacitance over a wide range of input voltage is much smaller which makes the frequency conversion weaker. Therefore, even though there are no Hopf bifurcations, the back-to-back structure may not be an optimum choice for frequency multiplication. The conversion efficiency can be improved by biasing away from zero volts because of the C-V asymmetry presented to the input signal.

In the next two sections, the numerical part of the work is outlined. First, we provide some background information on the harmonic balance formulation of the circuit.

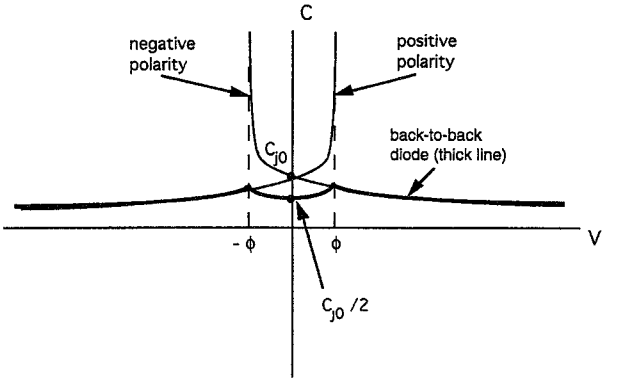

Fig. 5. The C-V curves of a positive polarity diode, negative polarity diode, and a series combination of two back-to-back diodes.

III. Harmonic Balance Formulation

An arbitrary network consisting of resistive and dynamical elements, linear or nonlinear, can be broken down by the piecewise method [14] into linear and nonlinear subcircuits. This topology is computationally efficient since in the microwave realm, the number of nonlinear elements is much less than the linear part. Consequently, the number of equations are reduced to the number of nonlinear elements in the circuit, regardless of the number of nodes. In addition, the information about the linear network can be stored in the computer in the form of Y parameters and do not have to be recalculated at every iteration during the nonlinear analysis. The equations at the junction of the linear-nonlinear network can be solved in frequeny or time domain. The time-domain approach provides both transient and steady-state information unlike the frequency-domain approach which provides only the latter. However, in the time domain some distributed circuits such as the radial stub are nearly impossible to model, especially its dispersive nature. Moreover, widely separated input frequencies and time constants pose additional numerical problems.

If the transient information is not as significant to the designer, then the simplest and computationally inexpensive method to obtain just the steady-state information is to solve the equations in the frequency domain. Hence, the information on the linear network is kept in the frequency domain. Since the nonlinear network is generally modeled accurately in the time domain, the data is Fourier transformed and its respective harmonics are equated with that of the linear network. This process is repeated continually under a root-finding scheme until convergence is achieved. This method is known as the harmonic balance analysis.

To illustrate this analysis, without loss of generality, the nonlinear network can be represented as a parallel combination of nonlinear resistor and nonlinear capacitor shown in Fig. 6. This assumption is reasonable since, for all practical purposes, a nonlinear inductance is rare in microwave circuits. Moreover, this nonlinear network happens to be a good representation of any diode, although the nonlinear capacitance for a Si *pn* junction diode is of two types, depletion and diffusion. This fact is incorporated in the formulation to perform harmonic balance and stability analysis of the frequency doubler.

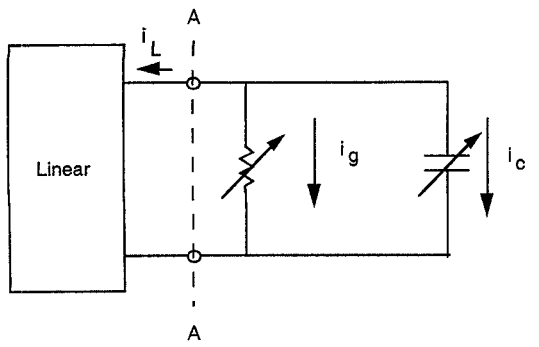

Fig. 6. A typical linear-nonlinear network configuration for multipliers.

The current into the linear network can be stated as the convolution between the admittance impulse response and the voltage across the terminal

$$i = y \otimes v. \tag{1}$$

We use the standard convention of employing capital letters to denote frequency domain quantities and reserve small letters for time domain quantities. Since the voltage and current waveforms are periodic, they can be represented by Fourier series

$$v(t) = \sum_k V_k e^{jk\omega_0 t} \tag{2a}$$

$$i(t) = \sum_k I_k e^{jk\omega_0 t} \tag{2b}$$

where $\sum_k$ represents summation of k from minus infinity to plus infinity. The admittance impulse response is an aperiodic function of time which necessitates the use of Fourier transform to convert to frequency domain. The Fourier transform of a sum of exponentials in time is a sum of scaled delta functions shifted in frequency. Consequently, the Fourier transform of (1) becomes

$$y \otimes v \Leftrightarrow \sum_k Y(k\omega_0) \cdot V_k \cdot \delta(\omega - k\omega_0) \tag{3}$$

and the inverse Fourier transform of (3) follows

$$y \otimes v = \sum_k Y(k\omega_0) \cdot V_k \cdot e^{jk\omega_0 t}. \tag{4}$$

Hence, the *harmonic balance* equation at the junction A-A in Fig. 6 can be written in the form of Fourier series in terms of the kth component as

$$E(V_k) = I_{d,k} + I_{c,k} + Y(k\omega_0) \cdot V_k. \tag{5}$$

The function E_k is called the error function. A standard procedure for solving a nonlinear set of equations such as (5) is through some iterative method. The most efficient method to-date is the Newton Raphson approach. In this method, we need to use the Jacobian of (5) which is given by

$$\frac{\partial \bar{F}}{\partial \bar{V}} = \frac{\partial \bar{I}_d}{\partial \bar{V}} + j\tilde{\Omega}\frac{\partial \bar{Q}}{\partial \bar{V}} + \tilde{Y}. \tag{6}$$

The bar represents a vector form and the tilda a matrix form. In essence, (6) is a sum of conductance, capacitive reactance, and Y-parameter matrices, respectively. And symbolically, it can be written, respectively, as

$$\tilde{J} = \tilde{G} + j \cdot \tilde{\Omega} \cdot \tilde{C} + \tilde{Y}. \tag{7}$$

In the conductance and capacitive reactance matrices, the off-diagonal elements parallel to the diagonal are similar in magnitude but opposite in phase, and the magnitude diminishes as we travel toward the corners of the matrix. Although, the above derivation is done in complex domain, this is usually numerically implemented in real quantities as in Kundert *et al.* [15] to reduce memory size requirement and improve the efficiency of its LU decomposition.

The convergence problems can be considerably alleviated by the piecewise parametrization in [16] and the newton-update norm-based damping strategy [17]. Now, we are ready to formulate the stability equations for a generic practical microwave circuit.

IV. Stability Formulation

Starting from Kurokawa's circuit in [4], it is restructured as depicted in Fig. 7 to enable the current to be formulated in terms of admittance parameters as

$$[Y(\omega_i) + Y(A)] \cdot V = I_S. \tag{8}$$

Allowing the nonlinear current to be stated as a nonlinear function of voltage, we have

$$Y(\omega_i) \cdot V + F(V) = I_S. \tag{9}$$

The inverse Fourier transform converts (9) into time domain. Now if we abandon complete generality and instead use a practical approach to describe the nonlinear network, it can be modeled by a parallel combination of a nonlinear resistor and a nonlinear capacitor as depicted in Fig. 6. Then the time-domain version of (9) becomes

$$y \otimes v + i_d + \frac{dq}{dt} = i_s. \tag{10}$$

To investigate the stability properties of (10), we take a first order Taylor series expansion of (10) around a steady state solution v_0,

$$y \otimes (v_0 + \Delta v) + i_d(v_0 + \Delta v) + \frac{dq(v_0 + \Delta v)}{dt} = 0 \tag{11}$$

and equate the steady state terms to zero to obtain

$$y \otimes \Delta v + \frac{di_d}{dv}\Delta v + \frac{d}{dt} \cdot \frac{dq}{dv} \cdot \Delta v = 0. \tag{12}$$

A steady state solution of (10) is a periodic function and can be represented in terms of a Fourier series

$$v_0 = \sum_k V_k \cdot e^{jk\omega_0 t}. \tag{13}$$

In order to perform stability analysis, the ansatz for (12) can be chosen to be a growing perturbation of the form

$$\Delta v = \mathrm{Re} \sum_k \{\Delta V_k \cdot e^{st}\} \cdot e^{jk\omega_0 t} \tag{14}$$

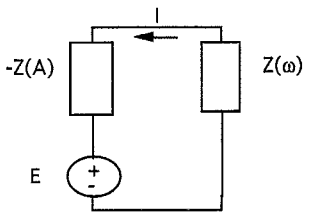

Fig. 7. Kurokawa's equivalent circuit for stability analysis.

where $s = \sigma + j\omega$ and $\sigma > 0$. The above equation is not a Fourier series, although it may resemble so, but instead it is a perturbation of the coefficients of the Fourier series in amplitude and frequency.

Substitution of (14) into (12) leads to a convolution, conductance, and a capacitive-reactance matrix term. The conductance term is

$$\frac{di_d}{dv} \cdot \Delta v = \left[\sum_k \frac{dI_{d,k}}{dV_1} \cdot e^{j(k-l)\omega_0 t}\right] \cdot \sum_l \Delta V_l \cdot e^{st} \cdot e^{jl\omega_0 t} = \sum_k \sum_l G_{k-l} \cdot e^{(s+jk\omega_0)t} \cdot \Delta V_l \quad (15)$$

and the capacitance term is

$$\frac{di_c}{dv} \cdot \Delta v = \sum_k \sum_l (s + jk\omega_0) \cdot C_{k-l} \cdot e^{(s+jk\omega_0)t} \cdot \Delta V_l. \quad (16)$$

The derivation of the convolution term here uses a different approach from what has been presented in earlier work [3, 4]. First, we can write the time domain convolution as the inverse Fourier transform of the Fourier transform of itself

$$y(t) \otimes \Delta v = \mathbf{F}^{-1}[\mathbf{F}\{y(t) \otimes \Delta v\}]. \quad (17)$$

Substitution of (14) into (17) and noting that the Fourier transform is a linear function, it follows that

$$y \otimes \Delta v = \sum_k \Delta V_k \cdot \mathbf{F}^{-1}[Y(\omega) \cdot \mathbf{F}\{e^{(s+jk\omega_0 t)}\}]. \quad (18)$$

The growing exponential in the above equation poses a problem. The Fourier transform of this type of function cannot be taken ordinarily since the integrand of the Fourier integral becomes unbounded [18]. However, by defining the transform variable to be complex, we can remove this singularity

$$\omega = \omega_1 + j\omega_2. \quad (19)$$

The complex Fourier transform can be expressed by

$$\int_{-\infty}^{\infty} e^{st} \cdot e^{-j\omega t} \cdot dt = \int_{-\infty}^{\infty} e^{(\sigma+\omega_2)t} \cdot e^{(\omega-\omega_1)t} dt. \quad (20)$$

The integrand blows up unless we set $\omega_2 = -\sigma$, which implies that the value of the integral is mapped onto a point in the complex plane in the frequency domain

$$\mathbf{F}\{e^{st}\} \equiv \delta(\omega_1 - \omega + j(\omega_2 + \sigma)). \quad (21)$$

When taking the inverse Fourier transform the contour is taken along the ω_1 axis with an $\omega_2 = -\sigma$ offset on the imaginary axis as shown in Fig. 8. Hence, we can define the inverse Fourier transform to be

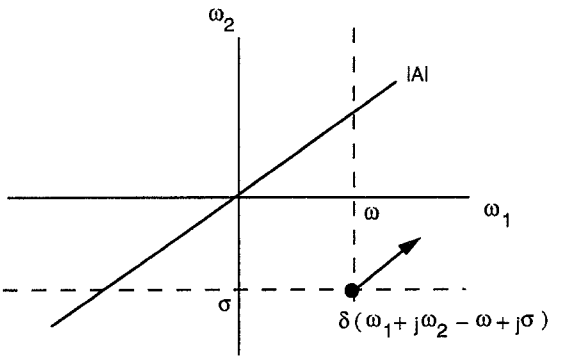

Fig. 8. The mapping of e^{st} in the the s-plane.

$$\mathbf{F}^{-1}\{\delta(\omega_1 + j\omega_2 - \omega + j\sigma)\} \equiv e^{st}. \quad (22)$$

Hence, it follows that $Y(\omega)$ evaluated at the location of delta function is

$$y \otimes \Delta v = Y(k\omega_0 - js) \cdot \sum_k \Delta V_k \cdot e^{(s+jk\omega_0)t}. \quad (23)$$

Substitution of (13), (14), and (23) into (12) leads to

$$\sum_k \sum_l [G_{k-l} + (s + \Omega_{k,l}) \cdot C_{k-l} + Y(\Omega_{k,l} - js)] \times \Delta V_k \cdot e^{(s+jk\omega_0)t} = 0 \quad (24)$$

where

$$\Omega_{k,l} = \begin{Bmatrix} k\omega_0, & \text{for } k = l \\ 0 & \text{otherwise} \end{Bmatrix}.$$

The above equation is a multiplication of a discrete value matrix with an exponential function varying continuously in time. In order for (24) to hold for all time it is necessary for the discrete part to be zero. Therefore, in the matrix notation form, it follows that

$$[\tilde{G} + (s + \tilde{\Omega}) \cdot \tilde{C} + \tilde{Y}(\tilde{\Omega} - js)] \cdot \overline{\Delta V} \equiv \tilde{J}_S \cdot \overline{\Delta V} = \bar{0}. \quad (25)$$

This is a generalized eigenvalue equation similar to Rizzoli's formulation except for its simplicity and practicality, and unlike in Kurokawa's case can be directly subjected to a Nyquist stability criterion and applicable to large signals. The terms inside the square brackets are alike that of the Jacobian of the harmonic balance except for the inclusion of the 's' variable; hence, it's called here the Stability Jacobian and is represented by $\tilde{J}_S$.

In order to circumvent the difficulty of finding the eigenvalues, Kurokawa [4] and Rizzoli *et al.* [5] chose to use the Nyquist approach to extract the stability properties of the system. Following the same approach the determinant of $\tilde{J}_S$ is plotted from $[0, \infty]$. The linear network is assumed to be a passive dissipative network. Hence, its admittance function does not have any poles on the imaginary axis. And due to the absence of nonlinear inductors in the formulation, $\det(\tilde{J}_S)$ cannot have any poles other than only one at infinity.

The number of zeros on the imaginary axis can be found directly from the plot of $\det(\tilde{J}_S)$. However, the existence

of zero is physically and numerically impossible. A zero implies that the eigenvalue is a nonhyperbolic point and, hence, nongeneric. Hence, it will degenerate to a hyperbolic point either on the LHS or RHS of the s-plane under a small perturbation. The source of perturbation in a physical system can be from a noise source or, numerically, appear as round-off and truncation errors. As a result the existence of a zero determinant is numerically impossible and physically unobservable. However, if a zero is to exist the Jacobian will become singular and not numerically converge. It follows then that this zero will be numerically difficult to find unless a specific algorithm is set up to detect changes in the condition number of the Jacobian. Thus, if the Jacobian can be taken, the contribution of zeros to the number of encirclements can be discounted. The periodic property of $\det(\tilde{J}_S)$ with respect to $s = j\omega$ for large number of harmonics is derived in [5]. Following [5], the $\det(\tilde{J}_S)$ is modified by a factor of $\exp(-\pi s/\omega_0)$ to remove the singularity at infinity. Moreover, because of its conjugacy and its periodic properties for large number of harmonics, the $\det(\tilde{J}_S)$ needs to be plotted only in the range $[0, \omega_0/2]$ to extract the stability information. The criterion for instability then becomes simply

$$N_0 = Z \Rightarrow \text{ stable if and only if } N_0 = 0 \qquad (26)$$

where N_0 is the total number of encirclements of the origin, and Z is the number of unstable zeros on the right-hand plane (RHP) of the s-plane.

Fig. 9 depicts the theoretical and experimental curves of the output power of the frequency doubler at 10 GHz with the bias level held fixed at -2.0 V. The experimental Hopf bifurcation point observed at the input power level of 11 dBm confirms well with the theoretical estimate of 10.4 dBm. At the bifurcation point, a pair of zeros crosses over the imaginary axis to the RHP. However, the magnitude of the self-oscillation is very small. At this input power level, a second pair of zeros crosses over to the RHP and the magnitude of the multi-tone spectral lines increases dramatically. The measured output power becomes considerably higher than the calculated curve. A likely cause is that the negative resistance of the diode increases and acts as a parametric amplifier to the input signal. Since this is not taken into account in this single-tone analysis, the experimental curve is higher than the numerical curve. To construct the numerical curve accurately, it is necessary to resort to a complete multi-tone harmonic balance analysis. This is especially true close to the 12 dBm point since the mixing products become considerably larger.

A. Numerical Verification

The primary Hopf bifurcation can be predicted based on a single tone stability analysis as described in Section II. To determine if the cause of Hopf bifurcation is due to the recombination time delay, the diffusion capacitance was modeled explicitly in terms of the minority carrier lifetime, τ, of the diode as

$$C = \tau \cdot \frac{dI(V)}{dt} \qquad (27)$$

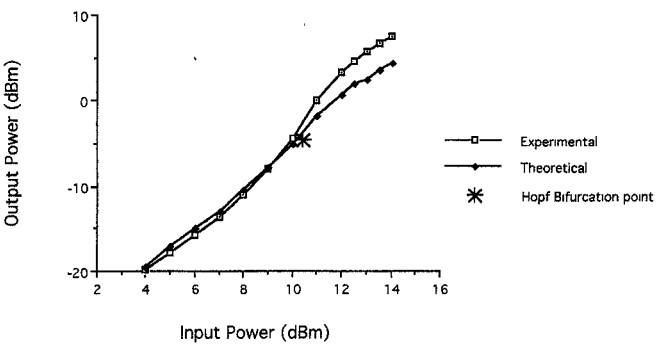

Fig. 9. Theoretical and measured output power of doubler and location of Hopf bifurcation point with input power variation.

where the current $I(v)$ is given by the familiar Shockley diode equation. According to the manufacturer specifications of the diode (Alpha DVA6735), τ is about 10 ns. With this value the predicted bifurcation point is about 1–1.5 dB off from the experimental result as mentioned earlier, where the bifurcation parameter used is the input power level. This discrepancy is acceptable since quasi-static models used in simulating the linear part of the circuit have limited accuracy bandwidth. When this delay is made negligibly small, for example $\tau = 6$ ps, no numerical Hopf bifurcation appears. This is because very little charge is stored in 3/100th period of the input signal, T ($f = 5$ GHz). When the delay is made bigger to about $3/10T$, then Hopf bifurcation registers, although at a higher bifurcation parameter value. As the delay is made closer to its norm of 10 ns the occurence of Hopf bifurcations registers closer to the experimentally observed value. No change in the Hopf point was observed if the delay was changed by a factor of 10 about its norm; hence, the predicted Hopf point is quite stable within manufacturer tolerances of the delay. Thus, the dependence of Hopf bifurcation on the minority carrier lifetime of the junction diode is clear from the above numerical results. Furthermore, this single-tone stability analysis can still be used for further increment of input power or bias level to detect a secondary Hopf bifurcation, even after the initial one. This is valid only in this case, since it is apriori known experimentally that the spurious tones were about 40 dB below the 10 GHz spectral output and, therefore, can be neglected; hence, a multi-tone analysis is not required. Numerically and experimentally, a secondary Hopf bifurcation occurs within 1.2 dB increase in the input power level (bifurcation parameter) showing that the system does bifurcate into a three-frequency quasi-periodic regime. In [13], it has been theoretically and experimentally proven that when a system enters a three-frequency quasi-periodic regime it has the potential to disintegrate to chaos. In chaos literature, it has been numerically shown to occur for three-order autonomous circuits [19], but to prove its occurence in complex circuits such as the frequency doubler is difficult and has not yet been done. Hence, the best we have numerically achieved is to determine when the system goes into a three-frequency regime.

B. Piecewise Stability Analysis

The piecewise topology is essentially a division of an arbitrary circuit into linear and nonlinear subcircuits. This network

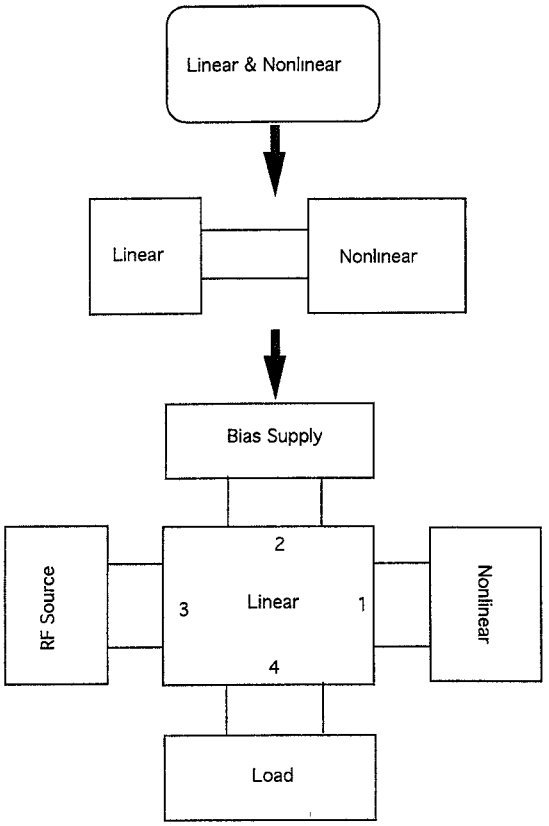

Fig. 10. The piecewise stability analysis concept for multi-parameter bifurcation analysis.

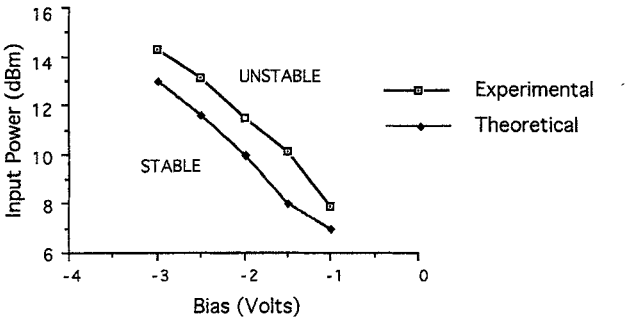

Fig. 11. A 2-parameter global stability analysis of microwave doubler for input signal power and bias variation.

structure reduces the number of equations considerably in the case of fewer nonlinear elements which is a norm in practical microwave circuits. The same piecewise idea is implemented in this paper for multiparameter stability analysis; however, this time it is for a different purpose. For a microwave engineer, it is desirable to have a global stability chart for all kinds of parametric variation such as the input power, the bias level, the load, and the tuning stub of the circuit. For example, if a global stability analysis based on the load variation is to be carried out, it would be necessary to recalculate the Y-parameters of the linear circuit everytime the load conditions are changed. The frequencies for which the Y-parameters need to be calculated are given by $[\omega + \Omega_k]$ set where ω is in the range $[0, \omega_0/2]$ and Ω_k is a vector of $\pm K$ harmonics of the fundamental, ω_0. Numerically, the number of points for the range $[0, \omega_0/2]$ will vary depending on the nonlinearity and the narrowband characteristics of the circuit. Thus, it is obvious that a considerable amount of computational time can be saved if the recalculation of the Y-parameters for the frequency set is avoided. The achievable speed-up depends on the size of the Y-matrix and the number of bifurcation parameters.

The PSA concept follows [14]. However, the partitioning strategy of an arbitrary circuit discussed here is not restricted to nonlinear subcircuits, but extended as well to parametric subcircuits. The diagram in Fig. 10 describes this concept through an example. The input power, bias, and the load are chosen as representative parameters for which a global stability analysis may be desired. These parameters are then extracted from the linear subcircuit and placed into individual subcircuits. The resulting topology is a 4-port network instead of a 1-port network. If we identify port 4 as load, port 3 as the input signal, and port 2 as the bias, a harmonic balance equation can be written at port 1

$$\bar{I}_{\mathrm{NL}} = \bar{I}_1 = \{\tilde{Y}_{11} - \tilde{C} \cdot \tilde{Y}_{41}\}\bar{V}_1 + \{\tilde{Y}_{12} - \tilde{C} \cdot \tilde{Y}_{42}\}\bar{V}_2 + \{\tilde{Y}_{13}\tilde{C} \cdot \tilde{Y}_{43}\}\bar{V}_3 \tag{28}$$

where $\bar{I}_{\mathrm{NL}}$ is the current through the nonlinear element(s) of a single nonlinear device, $\tilde{Y}_{ij}$ is a matrix corresponding to ij ports of the linear network, and

$$\tilde{C} = \tilde{Y}_{14}\tilde{Z}_L\{\tilde{I} + \tilde{Y}_{44}\tilde{Y}_L\}^{-1}. \tag{29}$$

If we apply the Newton-Raphson method, we need the Jacobian of (1) which is of the form

$$\tilde{J} = \tilde{J}_{\mathrm{NL}} - \{\tilde{Y}_{11} - \tilde{C} \cdot \tilde{Y}_{41}\}. \tag{30}$$

The PSA concept was used to conduct a 2-parameter stability analysis of the doubler; the two parameters being the input power and the bias level.

In order to numerically obtain the 2-parameter bifurcation diagram, the circuit is separated into three ports consisting of the RF source, the bias source, and the nonlinear element, respectively. Further reduction of the network size comes from placing the bias and the RF source into one source vector as $V_s = [V_{\mathrm{DC}}, V_0, 0, \ldots, 0]$. As a result, the network size is now reduced by one dimension to a 2-port network. This 2-port network is simulated using MDS [20] and the Y-parameters obtained.

Fig. 11 plots the input power and bias levels for which Hopf bifurcation occurs. The theoretical and experimental bifurcation diagram are close to within 1–1.5 dB of input power level. This slight discrepancy could be due to inaccurate modeling of the passive elements at higher frequencies since quasi-static models in [20] were used. The linear characteristic of the curve in the bifurcation diagram is explained as follows. A dynamical negative resistance is set up whenever the diode is forward biased. Since the forward bias voltage is the sum of the bias and the sinusoidal source voltage, the two bifurcation parameters essentially behave as one. Hence, their relationship is linear.

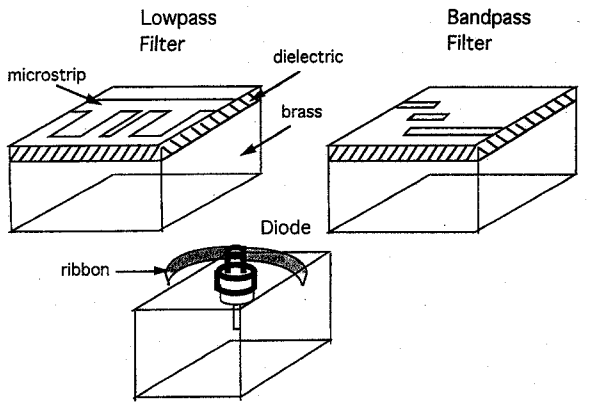

Fig. 12. A realization of the microwave frequency doubler circuit.

V. Frequency Doubler Design

The design of the doubler follows [1]. The data for the *pn* junction varactor Alpha DVA6735 used in our frequency doubler has the following parameters: $C_{j0} = 0.375$ pF, $\varphi = 0.52$ V, $V_b = -30.0$ V, $\gamma = 0.5$, and $R_s = 2.1\ \Omega$. The series resistance, R_s, is found from the cutoff frequency specified on the data sheet.

The matching networks are designed to be noninteracting. That is, the input matching network is designed to manifest an infinite impedance at the output frequency and vice versa to avoid RF signal leakage through the other port. Doublers are generally high-Q device and is difficult to achieve wideband operation. The matching network at the input is a lowpass filter and at the output is a bandpass filter with necessary tuning stubs on either port to achieve matching. The ends of the filters close to the diode are adjusted with a 50 Ω transmission line so that the impedance presented to the diode at their respective unwanted frequency is very high.

The two filters are mounted on separate brass blocks for rigidity and assembled together with the diode piece in the middle as depicted in Fig. 12. Two bond wires connect the diode to the two filters. The bond wires are quite long because the height of the diode is high. The bond wires should be as wide and thick and as short as possible to prevent radiation loss. One way of reducing the length of the bond wire is to lower the middle piece of brass block so that the head of the diode is aligned with the level of the microstrip. This can reduce the loss by as much as 2 dB.

A significant part in the large signal design of a varactor frequency doubler is to chart the instabilities of the circuit due to the bias and input power level variations. The bias and input power level conceptually are the same parameter that causes instabilities. It has been observed experimentally and numerically that as the combined level of the bias and the instantaneous RF input voltage level increases beyond a critical point, spurious oscillations occur. To counter these instabilities and yet still have high output power, the bias level can be set at a very low level (not beyond breakdown voltage) so that the input power can be high without resulting in any loss of stability.

The lowest conversion loss achieved was about 4.7 dB at 4.78 GHz input frequency. This value is reasonable considering the loss in the series resistance of the diode at all harmonics (recall that there are no idlers), through radiation from the circuit at 10 GHz, and in connectors.

The performance of a doubler can be enhanced by using faster varactor diodes (this has an inherent physical limitation), or majority carrier devices such as Schottky barrier or heterostructure diodes.

VI. Conclusion

We have predicted the arrival of spurious oscillation which leads to chaos in a doubler using the Hopf bifurcation concept and have confirmed experimentally the validity of our formulation to 1.5 dB. This finding helps the designer to locate the instabilities in the circuit for parametric variations such as the input power and the bias level.

The stability formulation presented in this work is simple, accurate and quite general to be used in all practical microwave circuits. The derivation is rigorous and uses the "complex" Fourier transform to achieve the same result obtained through intuitive mathematical treatment in previous work.

We have characterized the spurious oscillation in the microwave doubler circuit to be a quasi-periodic route to chaos as the system parameter (input power or bias level) is varied. The cause of the onset of this oscillation has been experimentally verified with a modified doubler circuit that does not exhibit bifurcation. In addition, the onset has been verified with the numerical simulation of the recombination delay parameter. The quasi-periodic path to chaos has also been numerically verified through a single-tone stability analysis.

Finally, the development of the piecewise stability analysis (PSA) technique allows the reduction of considerable computation time for performing multi-parameter stability analysis.

References

[1] S. A. Maas, *Nonlinear Microwave Circuits*. Norwood, MA: Artech House, 1988.
[2] S. M. Krakauer, "Harmonic generation, rectification, an lifetime evaluation with the step recovery diode," in *Proc. IRE*, July 1962, pp. 1665–1676.
[3] R. E. Collin, *Foundations of Microwave Engineering*, 2nd ed. New York: McGraw-Hill Inc., 1992, pp. 814–820.
[4] K. Kurokawa, "Injection locking of microwave solid-state oscillators," in *Proc. IEEE*, Oct. 1973, vol. 61, no. 10, p. 1398.
[5] V. Rizzoli and A. Lipparini, "General stability analysis of periodic steady-state regimes in nonlinear microwave circuits," *IEEE Trans. Microwave Theory Tech.*, vol. 33, no. 1, Jan. 1985.
[6] Several articles about chaos in *Proc. IEEE*, Special Issue on Chaotic Systems, Aug. 1987, vol. 75, no. 8.
[7] C. M. Glenn and S. Hayes, "Observation of chaos in a microwave limiter circuit," *IEEE Microwave and Guided Wave Lett.*, vol. 4, no. 12, Dec. 1994.
[8] M. I. Sobhy *et al.*, "Chaotic behavior of gunn oscillators," *21st European Microwave Symp.*, Stuttgart, Germany, Sept. 1991, vol. 1, p. 190.
[9] R. Seydel, *From Equilibrium to Chaos: Practical Bifurcation and Stability Analysis*. New York: Elsevier, 1988.
[10] E. R. Hunt, *Phys. Rev. Lett.*, vol. 49, no. 14, p. 1054, Oct. 1982.
[11] A. Azzouz *et al.*, "Transition to chaos in a simple nonlinear circuit driven by a sinusoidal voltage source," *IEEE Trans. Circuits Syst.*, vol. 30, no. 12, Dec. 1983.
[12] J. Testa *et al.*, "Comment on a driven nonlinear oscillator," *Phys. Rev. Lett.*, vol. 49, p. 1055, 1982.
[13] D. Ruelle and F. Takens, "On the nature of turbulence," *Commun. Math. Phys.* vol. 20, pp. 167–192, 1971.

[14] M. Nakhla and J. Vlach, "A piecewise harmonic balance technique for determination of periodic response of nonlinear systems," *IEEE Trans. Circuits Syst.*, vol. 23, no. 2, Feb. 1976.
[15] K. S. Kundert and A. Sangiovanni-Vincentelli, "Simulation of nonlinear circuits in the frequency domain," *IEEE Trans. Computer-Aided Design*, vol. CAD-5, pp. 521–535, Oct. 1986.
[16] V. Rizzoli *et al.*, "State-of-the-art harmonic-balance simulation of forced nonlinear microwave circuits by the piecewise technique," *IEEE Trans. Microwave Theory Tech.*, vol. 40, no. 1, Jan. 1992.
[17] H. R. Yeager and R. W. Dutton, "Improvement in norm-reducing newton methods for circuit simulation," *IEEE Trans. Computer-Aided Design*, vol. 8, no. 5, May 1989.
[18] G. F. Carrier *et al.*, *Functions of a Complex Variable: Theory and Technique*. New York: McGraw-Hill, 1966, p. 307.
[19] L. O. Chua *et al.*, "The double scroll family," *IEEE Trans. Circuits and Syst.*, vol. CAS-33, no. 11, pp. 1073–1117, Nov. 1986.
[20] *Microwave Design System*, Hewlett Packard, 1993.

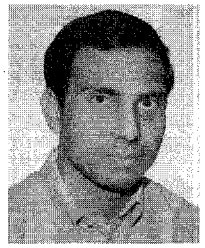

Saswata Basu was born February 11, 1970. He received the B.Eng. degree from Memorial University of Newfoundland, St. John's, Canada, and received the M.S. and Ph.D. degrees from UCLA in 1992 and 1994, respectively. His Master's thesis dealt with the design of a planar broadband mixer in a star configuration. His doctoral work involved characterizing, analyzing, and predicting stability of chaotic circuits such as frequency doublers.

He has been involved in designing phase-shifters, amplifiers, oscillators, SAW filters, RF detectors, and control circuits at Bell Northern Research, Ottawa, Canada from 1987 to 1991. He was a Teaching Assistant at UCLA for two years for various courses in electromagnetics. He joined Cascade Microtech Inc. in 1995 as a Senior Engineer and is currently working on next generation probes and calibration software.

Stephen A. Maas (S'80–M'83–SM'89–F'93) received the B.S.E.E. and M.S.E.E. degrees in electrical engineering from the University of Pennsylvania in 1971 and 1972, respectively, and the Ph.D. in electrical engineering from UCLA in 1984.

Since then, he has been involved in research, design, and development of low-noise and nonlinear microwave circuits and systems at the National Radio Astronomy Observatory (where he designed the receivers for the Very Large Array), Hughes Aircraft Co., TRW, the Aerospace Corp., and the UCLA Department of Electrical Engineering. He is now President and Principal Consultant of Nonlinear Technologies, Inc., specializing in the design of low-noise and nonlinear microwave components and systems, and minimization of distortion. He teaches periodically at UCLA, both regular and extension courses. He is the author of *Microwave Mixers*, (Norwood, MA: Artech House, 1986, and 1992) and *Nonlinear Microwave Circuits* (Norwood, MA: Artech House, 1988).

From 1990 until 1992 Dr. Maas was the editor of the IEEE TRANSACTIONS ON MICROWAVE THEORY AND TECHNIQUES and from 1990 to 1993 was an Adcom member and Publications Chairman of the IEEE MTT Society. He received the Microwave Prize in 1989 for his work on distortion in diode mixers. He is a Fellow of the IEEE.

Tatsuo Itoh, (S'69–M'69–SM'74–F'82) for a photograph and biography, see p. 1874 of the August 1995 issue of this TRANSACTIONS.